

PHENOMENOLOGY OF EUTECTIC LAMELLAR GROWTH

PHILIP LEE

ABSTRACT. In this paper I attempt to delimit the problem of using a phase field crystal model to study eutectic lamellar growth. I will discuss my simulations involving eutectic directional solidification for instability studies. By summarizing the seminal paper on lamellar eutectics by Jackson and Hunt, the simulations are put into context.

CONTENTS

Introduction	2
1. The Diffusion Equation	2
1.1. Lamellar Growth	2
1.2. Rod Growth	4
2. Average Curvatures	5
2.1. Lamellar interface	5
2.2. Rod-type interface	5
3. Thermodynamics	5
3.1. Equilibrium and Surface Thermodynamics.	5
3.2. Extremum Condition	6
4. Instability	7
4.1. Lamellar Fault	7
5. Phase Field Crystal Preliminary	8
5.1. Diffusion Equation	8
5.2. Correlation Function	8
5.3. Eutectic Phase Diagram	9
6. Simulations/Results	10
6.1. Setup	10
6.2. Lamellae Elimination	10
6.3. Lamellar Oscillations	11
7. Conclusion/Future Work	11
References	11

INTRODUCTION

This short paper will begin with a summary of the work by [JH], to include some basic details of e morphology in the classical sense. The experienced reader may skim through chapters 1 and 2 for this, although the model is quite interesting. The paper will conclude with attempts at creating a lamellar front using a phase field crystal model simulation, where topological instabilities will be simulated.

The striped eutectic phase is formed when the system is quenched through its eutectic point, below which no liquid phase can exist. This reaction is similar to spinodal decomposition in that the solutes tend to segregate, and solid-solid interfaces are formed. But whereas spinodal decomposition may be considered, in the language of phase field crystals, as a system which is (linearly) unstable to crystallization[EP], eutectic lamellar structure permeates, and persists through the sample. In this short paper, we will look at the seminal treatment of lamellar eutectic growth by Jackson and Hunt, and attempt to simulate 2D lamellar growth using the phase field crystal model. Time permitting, a qualitative summary of attempts to study the effect of crystalline mismatch with the propagation of instabilities may be included. This paper will conclude with some attempts at creating these instabilities.

1. THE DIFFUSION EQUATION

We begin by solving dynamical equations related to the configuration (reconfiguration) of solute, that are allowed to grow in a lamellar pattern, or as rods through a liquid phase. This will give us the necessary footing to understand the full evolution and interplay between regimes of growth, that occurs in the e phase. Along with the next chapter on curvature calculations, we will gain the necessary mathematical tools to tackle the problem in full.

1.1. Lamellar Growth. The basic treatment of a diffusion limited, directionally solidifying system starts with the following steady state equation¹,

$$0 = \nabla^2 C + \frac{v}{D} \frac{\partial C}{\partial z}$$

Where v is the velocity of the interface in the z (growth) direction. The boundary condition are:

$$C = C_E + C_\infty \text{ at } z = \infty$$

and due to the symmetry of the problem,

$$\frac{\partial C}{\partial x} = 0 \text{ at } x = 0 \text{ and } x = S_\alpha + S_\beta.$$

The conservation equations are,

$$\frac{\partial C}{\partial z} \Big|_{z=0} = -\frac{v}{D} C_0^\alpha$$

¹Reader may recognize this from the Kirkendall effect, and planar solidification found in many books on solidification and phase transformations. It is by admitting the convective term in the equation that is the source of instability in many systems. Although in [JH], this is not noted (explicitly) as the source of defects in the lamellar structure.

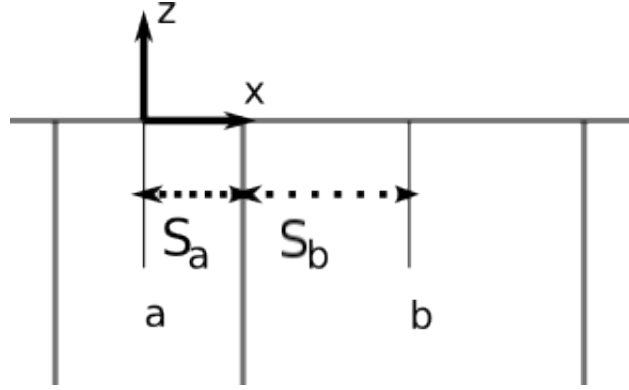


FIGURE 1. The setup of our first diffusion equation, z is the direction of growth.

for the α phase front, and

$$\left. \frac{\partial C}{\partial z} \right|_{z=0} = \frac{v}{D} C_0^\beta$$

for the β phase front, i.e. Fick's law for interface concentrations C_0^α and C_0^β . We are given the solution of the system of equations to be (discrete gaussian kernel),

$$C = C_E + C_\infty + B_0 e^{-\frac{v}{D}z} + \sum_{n=1}^{\infty} B_n \cos \frac{n\pi x}{S_\alpha + S_\beta} e^{-\frac{n\pi z}{S_\alpha + S_\beta}},$$

where we have assumed the diffusion length to be much smaller than the spacing $S_\alpha + S_\beta$. Using the boundary conditions to solve for the Fourier coefficients gives,

$$B_0 = \frac{C_0^\alpha S_\alpha - C_0^\beta S_\beta}{S_\alpha + S_\beta}, \text{ and}$$

$$B_n = \frac{2}{(n\pi)^2} (S_\alpha + S_\beta) \frac{v}{D} C_0 \sin\left(-\frac{n\pi z S_\alpha}{S_\alpha + S_\beta}\right).$$

The average composition in the liquid at the interface is,

$$\begin{aligned} \bar{C}_\alpha &= C_E + C_\infty + B_0 - \frac{1}{S_\alpha} \int_0^{S_\alpha} \sum_{n=1}^{\infty} B_n \cos\left(\frac{n\pi x}{S_\alpha + S_\beta}\right) dx \\ &= C_E + C_\infty + B_0 - \frac{2(S_\alpha + S_\beta)^2}{S_\alpha} \frac{v}{D} C_0 P. \end{aligned}$$

Similarly for,

$$\bar{C}_\beta = C_E + C_\infty + B_0 - \frac{2(S_\alpha + S_\beta)^2}{S_\beta} \frac{v}{D} C_0 P.$$

P is the series,

$$P = \sum_{n=1}^{\infty} \frac{1}{n\pi} \sin^2\left(\frac{n\pi S_\alpha}{S_\alpha + S_\beta}\right).$$

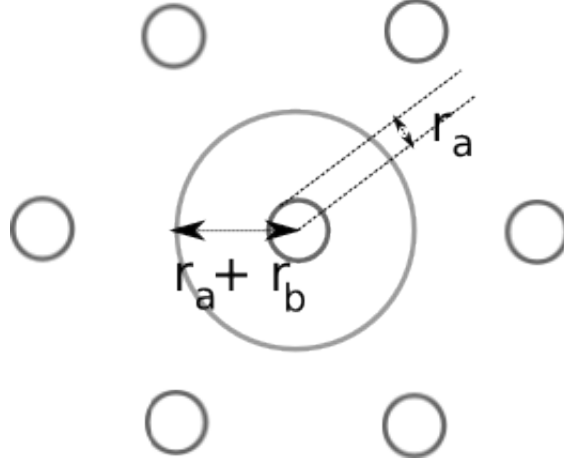


FIGURE 2. The variables referred in the equations. z is normal to the plane of the paper.

1.2. **Rod Growth.** We now derive the equation for rod growth through the sample. Using again the diffusion equation in the interface frame,

$$0 = \nabla^2 C + \frac{v}{D} \frac{\partial C}{\partial z}$$

where again z is the direction of growth, and v the rate of growth. With the same boundary conditions but in the not so tedious cylindrical coordinates²,

$$C = C_E + C_\infty \text{ at } z = \infty$$

$$\frac{\partial C}{\partial r} = 0 \text{ at } r = 0 \text{ and } r = r_\alpha + r_\beta,$$

$$\left. \frac{\partial C}{\partial z} \right|_{z=0} = -\frac{v}{D} C_0^\alpha$$

$$\left. \frac{\partial C}{\partial z} \right|_{z=0} = \frac{v}{D} C_0^\beta$$

where the second equation is for zero flux. The coordinate system used here neglects discrete symmetry.

The solution to this system of equations are the Bessel functions,

$$C = C_E + C_\infty + B_0 e^{-\frac{v}{D}z} + \sum_{n=1}^{\infty} A_n J_0\left(\frac{\gamma_n r}{r_\alpha + r_\beta}\right) e^{-\frac{n\pi z}{r_\alpha + r_\beta}},$$

where γ_n denotes the n^{th} root of the J_0 Bessel function and the coefficients A_n are derivable by the boundary conditions. For a more detailed account of the rod solutions, please see [JH].

²Much less tedious than paraboloidal.

2. AVERAGE CURVATURES

We will simply state the results by [JH] here. These calculations will be needed to calculate the Gibbs-Thomson effect.

2.1. Lamellar interface. The average curvature is given by,

$$\left\langle \frac{1}{r(x)} \right\rangle = \frac{1}{S_\alpha} \sin(\theta_\alpha),$$

where the geometric variables are as indicated in figure 1.

2.2. Rod-type interface. The average curvature is given by

$$\left\langle \frac{1}{\rho(x)} \right\rangle = \frac{-2}{(r_\alpha + r_\beta)^2 - r_\alpha^2} \sin(\theta_\beta),$$

calculated for an arbitrary surface of revolution of a curve in the first quadrant. θ_{beta} is the angle of the tangent at r_α .

3. THERMODYNAMICS

In this section we discuss the thermodynamics, and conjecture a growth condition for the system. The following will use the previous results to arrive at a qualitative behaviour of eutectics according to the model in [JH].

3.1. Equilibrium and Surface Thermodynamics. The equilibrium phase diagram shown in the figure, gives use the following undercooling,

$$\Delta T_C = m(C_E - C(x)), \text{ at the point } x \text{ along the interface.}$$

The Gibbs-Thompson effect gives us the capillary undercooling,

$$\Delta T_\sigma = \frac{a}{r(x)}.$$

[JH] ignores any kinetic contributions to the undercooling. Combining these effects, gives us the undercooling away from the eutectic at the interface. Thence,

$$T_E - T_i = \Delta T = \Delta T_C + \Delta T_\sigma$$

which remains constant across the solid-liquid interface.

Using the calculations from sections 1 and 2 we can now write,

$$\Delta T_\alpha = m_\alpha \left[C_\infty + B_0 + \frac{2v}{D} C_0 \frac{(S_\alpha + S_\beta)^2}{S_\alpha} P \right] + \frac{a_\alpha^L}{S_\alpha},$$

similarly for β ,

$$\Delta T_\beta = m_\beta \left[-C_\infty - B_0 + \frac{2v}{D} C_0 \frac{(S_\alpha + S_\beta)^2}{S_\alpha} P \right] + \frac{a_\beta^L}{S_\beta}.$$

where, a_i are the capillary lengths multiplied by $\sin(\theta_\beta)$ from section 2.

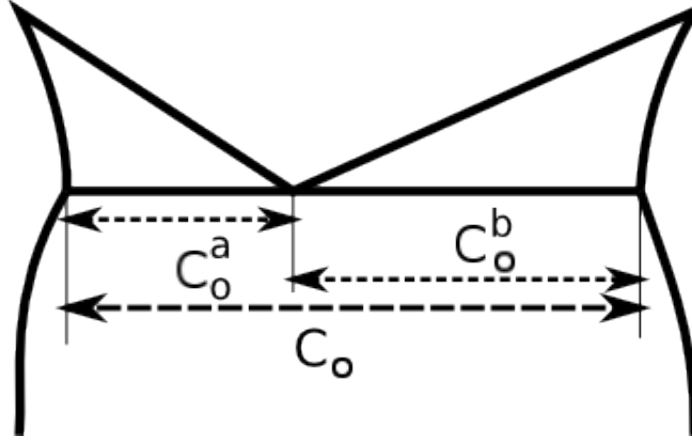


FIGURE 3. A typical eutectic phase diagram.

3.2. **Extremum Condition.** Nature, in this case will come in form of a constraint. We make the following ansatz:

”That the growth rate be the one which minimizes the undercooling”
or equivalently,

”for a given undercooling, the growth rate will be the fastest allowable.”

This conjecture is observed in many experiments and is originally proposed by Zener(1946), and formulated again by Tiller(1958) and Hillert(1960). By taking the derivative and minimizing, we get,

$$\lambda^2 v = \frac{a^L}{Q^L}$$

$$\frac{\Delta T^2}{v} = 4m^2 a^L Q^L$$

$$\Delta T \lambda = 2ma^L.$$

Where a^L , Q^L , and $\frac{1}{m}$ are,

$$a^L = 2(1 + \eta) \left(\frac{a_\alpha^L}{m_\alpha} + \frac{a_\beta^L}{\eta m_\beta} \right)$$

$$Q^L = \frac{P(1 + \eta)^2 C_0}{\eta D}$$

$$\frac{1}{m} = \frac{1}{m_\alpha} + \frac{1}{m_\beta}.$$

Similar equations hold for rod growth, in fact they are the same equations with the same function relationship to spacing and undercooling. I have included a schematic figure (4) from [JH] of the undercooling-spacing relationship for a given growth rate.

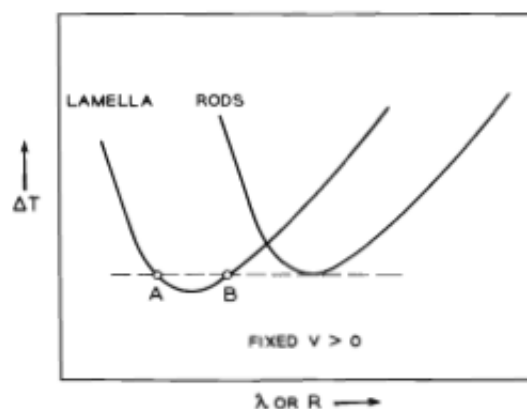


FIGURE 4. A rough schematic of rod and lamellar growth.

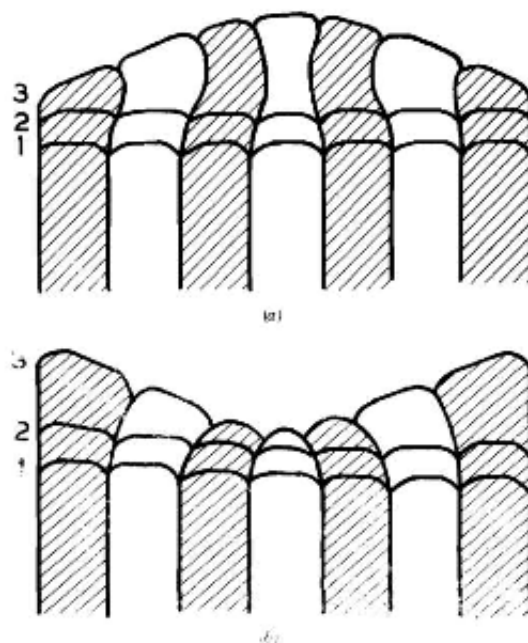


FIGURE 5. Two possible types of fluctuations.

4. INSTABILITY

4.1. **Lamellar Fault.** Two types of fluctuations may occur. These are shown in figure 5 originally from [JH].

The fluctuation depicted by the top illustration in figure 5, giving a deviation above the average spacing, will then be stabilized by a local decrease in undercooling. The bottom fluctuation, however is inherently unstable, as the lamellar will continue growing normal to the interface and will eventually impinge on each other, eventually changing the topology of the lamellar pattern. When such instability

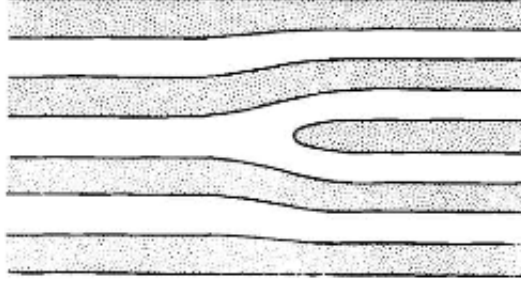


FIGURE 6. A lamellar fault. Growth direction is normal to the plane of the paper

occurs, it will be manifested like in figure 6 by [JH]. It is called a lamellar fault. It is said that the tip of the fault will follow the eutectic rod growth rate. Depending on the local deviation from the extremum spacing, the fault will move through the sample due to the uneven depression of the growth front caused by the instabilities in figure 5. In addition, these fault will only form on eutectic sub-grain boundaries as it is not very likely to occur homogeneously in the bulk.

5. PHASE FIELD CRYSTAL PRELIMINARY

This will be a summary of [EP].

5.1. Diffusion Equation. We begin with the functional diffusion equation, which is a general quality of material systems, in order to explain the phase field crystal model. From now on, phase field crystal will be referred to as PFC. A concentration C and a density field n in a binary alloy are coupled via the following two diffusion equations in the Gibbs free energy \mathcal{F} ,

$$\begin{aligned}\frac{\partial n}{\partial t} &= \vec{\nabla} \cdot \left\{ M_1 \nabla \frac{\delta \mathcal{F}}{\delta n} \right\} + \vec{\nabla} \cdot \left\{ M_2 \vec{\nabla} \frac{\delta \mathcal{F}}{\delta C} \right\} \\ \frac{\partial C}{\partial t} &= \vec{\nabla} \cdot \left\{ M_1 \nabla \frac{\delta \mathcal{F}}{\delta n} \right\} + \vec{\nabla} \cdot \left\{ M_2 \vec{\nabla} \frac{\delta \mathcal{F}}{\delta C} \right\}\end{aligned}$$

where M_1 and M_2 are the mobilities of the species normalized to atomic densities. The concentrations may be found given atomic volumes of the species. Finally, these dynamic equations may be discretized to create a time-stepped evolution equation.

5.2. Correlation Function. The free energy \mathcal{F} assumed in the PFC model has the following formal functional dependence on the density field,

$$\frac{\mathcal{F}}{k_B T} = \int_{\mathcal{V}} d\vec{x} \ln\left(\rho\left(\frac{\vec{r}_i}{\rho_l}\right)\right) - \sum_{n=2}^{\infty} \frac{1}{n!} \int_{\mathcal{V}} \prod_{i=1}^n d\vec{r}_i \delta\rho(\vec{r}_i) C_n(\vec{r}_1, \vec{r}_2, \dots, \vec{r}_n).$$

Where the functions C_n are the n -point correlation functions defined by,

$$C_n(\vec{r}_1, \vec{r}_2, \dots, \vec{r}_n) \equiv \frac{\delta^n \Phi}{\prod_{i=1}^n \delta\rho(\vec{r}_i)},$$

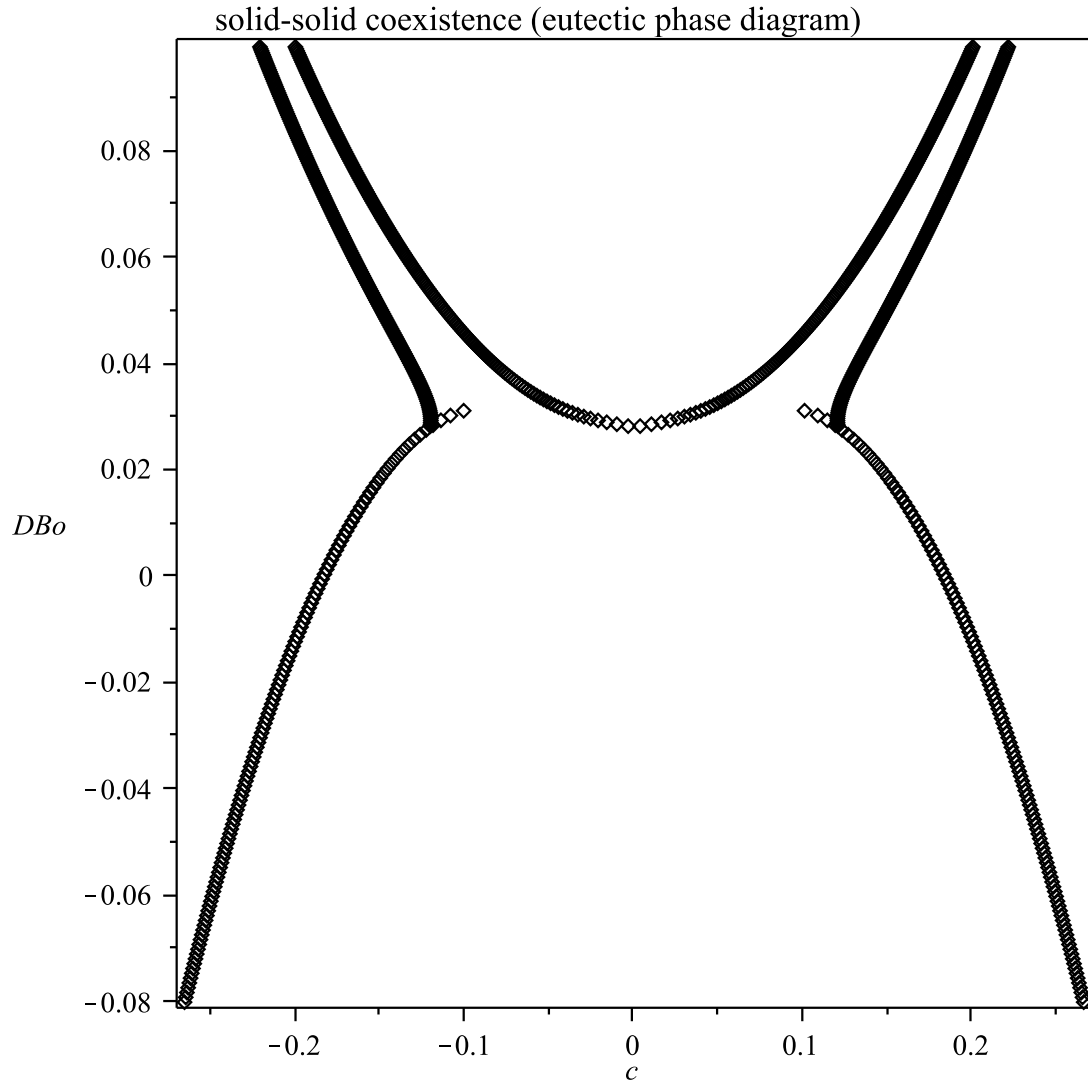


FIGURE 7. The vertical component is the "temperature" variable. The eutectic is at $DB_0 = 0.028$.

and Φ is the total potential energy related to a configuration of atoms (density field). It turns out that by truncating the series at the two-point correlation function, there is a characteristic periodicity where it is highly correlated. This is what the word '*crystal*' denote in pfc. The advantages of this '*crystal*' model is that it allows for strain, and elastic effects naturally.

5.3. Eutectic Phase Diagram. The concentration solutions of the common tangents to the free energy, the phase diagram, is given by figure 7, created by [ACSR]. The lines represent phase boundaries.

6. SIMULATIONS/RESULTS

6.1. **Setup.** A 2D pfc model simulation was set up such that there is a temperature gradient along one of its directions. The gradient is made in such a way that the undercooling temperature is at one end and then increases for the rest of the simulation box. The boundaries are set to have periodic boundary conditions, in both the lateral the direction and the vertical. A two phased seed was initially put in the undercooled end and allowed to solidify as the gradient is moved. Soon after the simulations began the system relaxes into some contact angle at the tri-junction.

6.1.1. *Stable Lamellar.* A few simulations were made under stable lamellar growth conditions. It was achieved with those conditions in the first column of table 1. Reader may find a movie of the simulation in the folder called stable and play the movie directionalgrowth.mov. However a finer spacing was achieved when the interface speed was increased $5\times$. Due to the periodic boundary, the stripes were diagonal in-order fulfill the proper spacing within the simulation box. In the density movie, the region where white dots appear in a roughly hexagonal array is the solid.

Variable	Stable	Finer Spacing
Initial conditions	2 stripes	2 stripes
Undercooling (DB_0)	0.022	0.022
Interface speed	1.3×10^{-4}	6.7×10^{-4}

TABLE 1. Stable Conditions

6.2. **Lamellae Elimination.** Here are the results for unstable lamellar growth.

Variable	Elimination	Elimination	Elimination
Initial conditions	4 stripes	8 stripes	8 stripes
Undercooling (DB_0)	0.022	0.022	0.016
Interface speed	6.7×10^{-4}	6.7×10^{-4}	6.7×10^{-4}

TABLE 2. Elimination Instability

For those parameters of directional solidification, the first column provides conditions that are *'almost'* stable for a 4 striped phase. For both simulation runs where there were 8 stripes present in the initial conditions, they quickly redistribute solute into a 4 striped phase after which they exhibit a defect, where they return to the stable 2 striped phase. The run with a smaller undercooling gives a very unstable wavy 4 striped phase before lamellae elimination. It suggests, as in [JH], undercooling dependence of lamellar structures³.

³This dependence on undercooling (specifically constitutional undercooling) is of course the basis of the famed Mullins-Sekerka linear instability analysis.

6.3. Lamellar Oscillations. Some phase field models [PF, 3D] have produced oscillations in the lamellar structure; that has yet to be explored in my studies. However, it may be safe to conjecture that it may appear in 2D simulations given a striped initial condition where one phase had advanced further than the other. This has been shown in a phase field simulation in [PF], with a perturbed interface. It may be now relevant to remark, that the pfc simulation used, though within its formalism, does not simulate thermal fluctuations. It was unclear to the writer whether [PF] allows for thermal fluctuations (dynamically, as a conserved field of temperature).

7. CONCLUSION/FUTURE WORK

Some correlation to [JH] has been seen. The pfc model shows roughly the right morphologies of eutectic instabilities in a directionally solidifying system. The code should be extended to 3-D to study the effects in [?, JH]ore completely. Due to the quick diffusion found in the simulation default, we are able to see the automatic relaxation into the correct contact angles at the tri-junction, this allows a more realistic simulation of surface energy effects, but may not be as useful for simulation of certain materials in bulk. The rather fast diffusion also allows after solidification solute redistribution, thus changing the patten. The boundary conditions may be changed to the no-flux to match those found in [PF, 3D], and compare the results with these phase field model.

REFERENCES

- [JH] K. A. Jackson, J. D. Hunt, Lamellar and rod eutectic growth. Transactions Of The Metallurgical Society Of Aime 236, 1129-1142 (1966).
- [EP] K.R. Elder, N. Provatas, J. Berry, P. Stefanovic, M. Grant, Phase-field crystal modeling and classical density functional theory of freezing. Physical Review B, Vol. 75, 064107 (2007).
- [CODE] J. Stolle, K.R. Elder, PFC simulation for binary alloy. Distributed with N, Provatas, K.R. Elder, Phase-Field Methods in Materials Science and Engineering. Wiley-VCH, 2010.
- [JJH] J. J. Hoyt, Phase Transformations. McMaster Innovation Press (2010).
- [PF] R. Folch, M. Plapp, Quantitative phase-field modeling of two-phase growth. Physical Review E 72, 011602 (2005)
- [3D] A. Parisi et al., Three-dimensional phase-field simulations of eutectic solidification and comparison to *in situ* experimental observations. TMS.
- [ACSR] J. Stolle, H. Humadi, N. Ofori-Opoku, Maple calculations based on [EP]